EUROPEAN ORGANIZATION FOR NUCLEAR RESEARCH

CERN–EP-2000-133

11 July 2000

Search for neutralino pair production at $\sqrt{s} = 189$ GeV

DELPHI Collaboration

Abstract

A search for pair-production of neutralinos at a LEP centre-of-mass energy of 189 GeV gave no evidence for a signal. This limits the neutralino production cross-section and excludes regions in the parameter space of the Minimal Supersymmetric Standard Model (MSSM).

(Submitted to Eur.Phys.J)

P.Abreu[22], W.Adam[51], T.Adye[37], P.Adzic[12], I.Ajinenko[43], Z.Albrecht[18], T.Alderweireld[2], G.D.Alekseev[17], R.Alemany[9], T.Allmendinger[18], P.P.Allport[23], S.Almehed[25], U.Amaldi[29], N.Amapane[46], S.Amato[48], E.G.Anassontzis[3], P.Andersson[45], A.Andreazza[28], S.Andringa[22], N.Anjos[22], P.Antilogus[26], W-D.Apel[18], Y.Arnoud[15], B.Åsman[45], J-E.Augustin[24], A.Augustinus[9], P.Baillon[9], A.Ballestrero[46], P.Bambade[9,20], F.Barao[22], G.Barbiellini[47], R.Barbier[26], D.Y.Bardin[17], G.Barker[18], A.Baroncelli[39], M.Battaglia[16], M.Baubillier[24], K-H.Becks[53], M.Begalli[6], A.Behrmann[53], Yu.Belokopytov[9], N.C.Benekos[32], A.C.Benvenuti[5], C.Berat[15], M.Berggren[24], L.Berntzon[45], D.Bertrand[2], M.Besancon[40], N.Besson[40], M.S.Bilenky[17], M-A.Bizouard[20], D.Bloch[10], H.M.Blom[31], L.Bol[18], M.Bonesini[29], M.Boonekamp[40], P.S.L.Booth[23], G.Borisov[20], C.Bosio[42], O.Botner[49], E.Boudinov[31], B.Bouquet[20], C.Bourdarios[20], T.J.V.Bowcock[23], I.Boyko[17], I.Bozovic[12], M.Bozzo[14], M.Bracko[44], P.Branchini[39], R.A.Brenner[49], P.Bruckman[9], J-M.Brunet[8], L.Bugge[33], P.Buschmann[53], M.Caccia[28], M.Calvi[29], T.Camporesi[9], V.Canale[38], F.Carena[9], L.Carroll[23], C.Caso[14], M.V.Castillo Gimenez[50], A.Cattai[9], F.R.Cavallo[5], Ph.Charpentier[9], P.Checchia[36], G.A.Chelkov[17], R.Chierici[46], P.Chliapnikov[9,43], P.Chochula[7], V.Chorowicz[26], J.Chudoba[30], K.Cieslik[19], P.Collins[9], R.Contri[14], E.Cortina[50], G.Cosme[20], F.Cossutti[9], M.Costa[50], H.B.Crawley[1], D.Crennell[37], J.Croix[10], G.Crosetti[14], J.Cuevas Maestro[34], S.Czellar[16], J.D'Hondt[2], J.Dalmau[45], M.Davenport[9], W.Da Silva[24], G.Della Ricca[47], P.Delpierre[27], N.Demaria[46], A.De Angelis[47], W.De Boer[18], C.De Clercq[2], B.De Lotto[47], A.De Min[9], L.De Paula[48], H.Dijkstra[9], L.Di Ciaccio[38], K.Doroba[52], M.Dracos[10], J.Drees[53], M.Dris[32], G.Eigen[4], T.Ekelof[49], M.Ellert[49], M.Elsing[9], J-P.Engel[10], M.Espirito Santo[9], G.Fanourakis[12], D.Fassouliotis[12], M.Feindt[18], J.Fernandez[41], A.Ferrer[50], E.Ferrer-Ribas[20], F.Ferro[14], A.Firestone[1], U.Flagmeyer[53], H.Foeth[9], E.Fokitis[32], F.Fontanelli[14], B.Franek[37], A.G.Frodesen[4], R.Fruhwirth[51], F.Fulda-Quenzer[20], J.Fuster[50], A.Galloni[23], D.Gamba[46], S.Gamblin[20], M.Gandelman[48], C.Garcia[50], C.Gaspar[9], M.Gaspar[48], U.Gasparini[36], Ph.Gavillet[9], E.N.Gazis[32], D.Gele[10], T.Geralis[12], L.Gerdyukov[43], N.Ghodbane[26], I.Gil[50], F.Glege[53], R.Gokieli[9,52], B.Golob[9,44], G.Gomez-Ceballos[41], P.Goncalves[22], I.Gonzalez Caballero[41], G.Gopal[37], L.Gorn[1], Yu.Gouz[43], J.Grahl[1], E.Graziani[39], G.Grosdidier[20], K.Grzelak[52], J.Guy[37], C.Haag[18], F.Hahn[9], S.Hahn[53], S.Haider[9], A.Hallgren[49], K.Hamacher[53], J.Hansen[33], F.J.Harris[35], S.Haug[33], F.Hauler[18], V.Hedberg[9,25], S.Heising[18], J.J.Hernandez[50], P.Herquet[2], H.Herr[9], O.Hertz[18], E.Higon[50], S-O.Holmgren[45], P.J.Holt[35], S.Hoorelbeke[2], M.Houlden[23], J.Hrubec[51], G.J.Hughes[23], K.Hultqvist[9,45], J.N.Jackson[23], R.Jacobsson[9], P.Jalocha[19], Ch.Jarlskog[25], G.Jarlskog[25], P.Jarry[40], B.Jean-Marie[20], D.Jeans[35], E.K.Johansson[45], P.Jonsson[26], C.Joram[9], P.Juillot[10], L.Jungermann[18], F.Kapusta[24], K.Karafasoulis[12], S.Katsanevas[26], E.C.Katsoufis[32], R.Keranen[18], G.Kernel[44], B.P.Kersevan[44], Yu.Khokhlov[43], B.A.Khomenko[17], N.N.Khovanski[17], A.Kiiskinen[16], B.King[23], A.Kinvig[23], N.J.Kjaer[9], O.Klapp[53], P.Kluit[31], P.Kokkinias[12], V.Kostioukhine[43], C.Kourkoumelis[3], O.Kouznetsov[17], M.Krammer[51], E.Kriznic[44], Z.Krumstein[17], P.Kubinec[7], M.Kucharczyk[19], J.Kurowska[52], J.W.Lamsa[1], J-P.Laugier[40], G.Leder[51], F.Ledroit[15], L.Leinonen[45], A.Leisos[12], R.Leitner[30], G.Lenzen[53], V.Lepeltier[20], T.Lesiak[19], M.Lethuillier[26], J.Libby[35], W.Liebig[53], D.Liko[9], A.Lipniacka[45], I.Lippi[36], J.G.Loken[35], J.H.Lopes[48], J.M.Lopez[41], R.Lopez-Fernandez[15], D.Loukas[12], P.Lutz[40], L.Lyons[35], J.MacNaughton[51], J.R.Mahon[6], A.Maio[22], A.Malek[53], S.Maltezos[32], V.Malychev[17], F.Mandl[51], J.Marco[41], R.Marco[41], B.Marechal[48], M.Margoni[36], J-C.Marin[9], C.Mariotti[9], A.Markou[12], C.Martinez-Rivero[9], S.Marti i Garcia[9], J.Masik[13], N.Mastroyiannopoulos[12], F.Matorras[41], C.Matteuzzi[29], G.Matthiae[38], F.Mazzucato[36], M.Mazzucato[36], M.Mc Cubbin[23], R.Mc Kay[1], R.Mc Nulty[23], G.Mc Pherson[23], E.Merle[15], C.Meroni[28], W.T.Meyer[1], E.Migliore[9], L.Mirabito[26], W.A.Mitaroff[51], U.Mjoernmark[25], T.Moa[45], M.Moch[18], K.Moenig[9,11], M.R.Monge[14], J.Montenegro[31], D.Moraes[48], P.Morettini[14], G.Morton[35], U.Mueller[53], K.Muenich[53], M.Mulders[31], L.M.Mundim[6], W.J.Murray[37], B.Muryn[19], G.Myatt[35], T.Myklebust[33], M.Nassiakou[12], F.L.Navarria[5], K.Nawrocki[52], P.Negri[29], S.Nemecek[13], N.Neufeld[51], R.Nicolaidou[40], P.Niezurawski[52], M.Nikolenko[10,17], V.Nomokonov[16], A.Nygren[25], V.Obraztsov[43], A.G.Olshevski[17], A.Onofre[22], R.Orava[16], K.Osterberg[9], A.Ouraou[40], A.Oyanguren[50], M.Paganoni[29], S.Paiano[5], R.Pain[24], R.Paiva[22], J.Palacios[35], H.Palka[19], Th.D.Papadopoulou[32], L.Pape[9], C.Parkes[9], F.Parodi[14], U.Parzefall[23], A.Passeri[39], O.Passon[53], T.Pavel[25], M.Pegoraro[36], L.Peralta[22], V.Perepelitsa[50], M.Pernicka[51], A.Perrotta[5], C.Petridou[47], A.Petrolini[14], H.T.Phillips[37], F.Pierre[40], M.Pimenta[22], E.Piotto[28], T.Podobnik[44], V.Poireau[40], M.E.Pol[6], G.Polok[19], P.Poropat[47], V.Pozdniakov[17], P.Privitera[38], N.Pukhaeva[17], A.Pullia[29], D.Radojicic[35], S.Ragazzi[29], H.Rahmani[32], A.L.Read[33], P.Rebecchi[9], N.G.Redaelli[29], M.Regler[51], J.Rehn[18], D.Reid[31], R.Reinhardt[53], P.B.Renton[35], L.K.Resvanis[3], F.Richard[20], J.Ridky[13], G.Rinaudo[46], I.Ripp-Baudot[10], A.Romero[46], P.Ronchese[36], E.I.Rosenberg[1], P.Rosinsky[7], T.Rovelli[5], V.Ruhlmann-Kleider[40], A.Ruiz[41], H.Saarikko[16], Y.Sacquin[40], A.Sadovsky[17], G.Sajot[15], L.Salmi[16], J.Salt[50], D.Sampsonidis[12], M.Sannino[14], A.Savoy-Navarro[24], C.Schwanda[51], Ph.Schwemling[24], B.Schwering[53], U.Schwickerath[18], F.Scuri[47], Y.Sedykh[17], A.M.Segar[35], R.Sekulin[37], G.Sette[14], R.C.Shellard[6], M.Siebel[53], L.Simard[40], F.Simonetto[36], A.N.Sisakian[17], G.Smadja[26], N.Smirnov[43], O.Smirnova[25], G.R.Smith[37], A.Sokolov[43], A.Sopczak[18], R.Sosnowski[52], T.Spassov[9], E.Spiriti[39], S.Squarcia[14], C.Stanescu[39], M.Stanitzki[18], K.Stevenson[35], A.Stocchi[20], J.Strandberg[45], J.Strauss[51], R.Strub[10], B.Stugu[4], M.Szczekowski[52], M.Szeptycka[52], T.Tabarelli[29], A.Taffard[23], O.Tchikilev[43], F.Tegenfeldt[49], F.Terranova[29], J.Timmermans[31], N.Tinti[5], L.G.Tkatchev[17], M.Tobin[23], S.Todorova[9], B.Tome[22], A.Tonazzo[9], L.Tortora[39], P.Tortosa[50], D.Treille[9], G.Tristram[8], M.Trochimczuk[52], C.Troncon[28], M-L.Turluer[40], I.A.Tyapkin[17], P.Tyapkin[25], S.Tzamarias[12], O.Ullaland[9], V.Uvarov[43], G.Valenti[9,5], E.Vallazza[47], C.Vander Velde[2], P.Van Dam[31], W.Van den Boeck[2], J.Van Eldik[9,31], A.Van Lysebetten[2], N.van Remortel[2], I.Van Vulpen[31], G.Vegni[28], L.Ventura[36], W.Venus[37,9], F.Verbeure[2], P.Verdier[26], M.Verlato[36],

L.S.Vertogradov[17], V.Verzi[28], D.Vilanova[40], L.Vitale[47], E.Vlasov[43], A.S.Vodopyanov[17], G.Voulgaris[3], V.Vrba[13], H.Wahlen[53], A.J.Washbrook[23], C.Weiser[9], D.Wicke[9], J.H.Wickens[2], G.R.Wilkinson[35], M.Winter[10], M.Witek[19], G.Wolf[9], J.Yi[1], O.Yushchenko[43], A.Zalewska[19], P.Zalewski[52], D.Zavrtanik[44], E.Zevgolatakos[12], N.I.Zimin[17,25], A.Zintchenko[17], Ph.Zoller[10], G.Zumerle[36], M.Zupan[12]

[1]Department of Physics and Astronomy, Iowa State University, Ames IA 50011-3160, USA
[2]Physics Department, Univ. Instelling Antwerpen, Universiteitsplein 1, B-2610 Antwerpen, Belgium
and IIHE, ULB-VUB, Pleinlaan 2, B-1050 Brussels, Belgium
and Faculté des Sciences, Univ. de l'Etat Mons, Av. Maistriau 19, B-7000 Mons, Belgium
[3]Physics Laboratory, University of Athens, Solonos Str. 104, GR-10680 Athens, Greece
[4]Department of Physics, University of Bergen, Allégaten 55, NO-5007 Bergen, Norway
[5]Dipartimento di Fisica, Università di Bologna and INFN, Via Irnerio 46, IT-40126 Bologna, Italy
[6]Centro Brasileiro de Pesquisas Físicas, rua Xavier Sigaud 150, BR-22290 Rio de Janeiro, Brazil
and Depto. de Física, Pont. Univ. Católica, C.P. 38071 BR-22453 Rio de Janeiro, Brazil
and Inst. de Física, Univ. Estadual do Rio de Janeiro, rua São Francisco Xavier 524, Rio de Janeiro, Brazil
[7]Comenius University, Faculty of Mathematics and Physics, Mlynska Dolina, SK-84215 Bratislava, Slovakia
[8]Collège de France, Lab. de Physique Corpusculaire, IN2P3-CNRS, FR-75231 Paris Cedex 05, France
[9]CERN, CH-1211 Geneva 23, Switzerland
[10]Institut de Recherches Subatomiques, IN2P3 - CNRS/ULP - BP20, FR-67037 Strasbourg Cedex, France
[11]Now at DESY-Zeuthen, Platanenallee 6, D-15735 Zeuthen, Germany
[12]Institute of Nuclear Physics, N.C.S.R. Demokritos, P.O. Box 60228, GR-15310 Athens, Greece
[13]FZU, Inst. of Phys. of the C.A.S. High Energy Physics Division, Na Slovance 2, CZ-180 40, Praha 8, Czech Republic
[14]Dipartimento di Fisica, Università di Genova and INFN, Via Dodecaneso 33, IT-16146 Genova, Italy
[15]Institut des Sciences Nucléaires, IN2P3-CNRS, Université de Grenoble 1, FR-38026 Grenoble Cedex, France
[16]Helsinki Institute of Physics, HIP, P.O. Box 9, FI-00014 Helsinki, Finland
[17]Joint Institute for Nuclear Research, Dubna, Head Post Office, P.O. Box 79, RU-101 000 Moscow, Russian Federation
[18]Institut für Experimentelle Kernphysik, Universität Karlsruhe, Postfach 6980, DE-76128 Karlsruhe, Germany
[19]Institute of Nuclear Physics and University of Mining and Metalurgy, Ul. Kawiory 26a, PL-30055 Krakow, Poland
[20]Université de Paris-Sud, Lab. de l'Accélérateur Linéaire, IN2P3-CNRS, Bât. 200, FR-91405 Orsay Cedex, France
[21]School of Physics and Chemistry, University of Lancaster, Lancaster LA1 4YB, UK
[22]LIP, IST, FCUL - Av. Elias Garcia, 14-1^{o}, PT-1000 Lisboa Codex, Portugal
[23]Department of Physics, University of Liverpool, P.O. Box 147, Liverpool L69 3BX, UK
[24]LPNHE, IN2P3-CNRS, Univ. Paris VI et VII, Tour 33 (RdC), 4 place Jussieu, FR-75252 Paris Cedex 05, France
[25]Department of Physics, University of Lund, Sölvegatan 14, SE-223 63 Lund, Sweden
[26]Université Claude Bernard de Lyon, IPNL, IN2P3-CNRS, FR-69622 Villeurbanne Cedex, France
[27]Univ. d'Aix - Marseille II - CPP, IN2P3-CNRS, FR-13288 Marseille Cedex 09, France
[28]Dipartimento di Fisica, Università di Milano and INFN-MILANO, Via Celoria 16, IT-20133 Milan, Italy
[29]Dipartimento di Fisica, Univ. di Milano-Bicocca and INFN-MILANO, Piazza delle Scienze 2, IT-20126 Milan, Italy
[30]IPNP of MFF, Charles Univ., Areal MFF, V Holesovickach 2, CZ-180 00, Praha 8, Czech Republic
[31]NIKHEF, Postbus 41882, NL-1009 DB Amsterdam, The Netherlands
[32]National Technical University, Physics Department, Zografou Campus, GR-15773 Athens, Greece
[33]Physics Department, University of Oslo, Blindern, NO-1000 Oslo 3, Norway
[34]Dpto. Fisica, Univ. Oviedo, Avda. Calvo Sotelo s/n, ES-33007 Oviedo, Spain
[35]Department of Physics, University of Oxford, Keble Road, Oxford OX1 3RH, UK
[36]Dipartimento di Fisica, Università di Padova and INFN, Via Marzolo 8, IT-35131 Padua, Italy
[37]Rutherford Appleton Laboratory, Chilton, Didcot OX11 OQX, UK
[38]Dipartimento di Fisica, Università di Roma II and INFN, Tor Vergata, IT-00173 Rome, Italy
[39]Dipartimento di Fisica, Università di Roma III and INFN, Via della Vasca Navale 84, IT-00146 Rome, Italy
[40]DAPNIA/Service de Physique des Particules, CEA-Saclay, FR-91191 Gif-sur-Yvette Cedex, France
[41]Instituto de Fisica de Cantabria (CSIC-UC), Avda. los Castros s/n, ES-39006 Santander, Spain
[42]Dipartimento di Fisica, Università degli Studi di Roma La Sapienza, Piazzale Aldo Moro 2, IT-00185 Rome, Italy
[43]Inst. for High Energy Physics, Serpukov P.O. Box 35, Protvino, (Moscow Region), Russian Federation
[44]J. Stefan Institute, Jamova 39, SI-1000 Ljubljana, Slovenia and Laboratory for Astroparticle Physics,
Nova Gorica Polytechnic, Kostanjeviska 16a, SI-5000 Nova Gorica, Slovenia,
and Department of Physics, University of Ljubljana, SI-1000 Ljubljana, Slovenia
[45]Fysikum, Stockholm University, Box 6730, SE-113 85 Stockholm, Sweden
[46]Dipartimento di Fisica Sperimentale, Università di Torino and INFN, Via P. Giuria 1, IT-10125 Turin, Italy
[47]Dipartimento di Fisica, Università di Trieste and INFN, Via A. Valerio 2, IT-34127 Trieste, Italy
and Istituto di Fisica, Università di Udine, IT-33100 Udine, Italy
[48]Univ. Federal do Rio de Janeiro, C.P. 68528 Cidade Univ., Ilha do Fundão BR-21945-970 Rio de Janeiro, Brazil
[49]Department of Radiation Sciences, University of Uppsala, P.O. Box 535, SE-751 21 Uppsala, Sweden
[50]IFIC, Valencia-CSIC, and D.F.A.M.N., U. de Valencia, Avda. Dr. Moliner 50, ES-46100 Burjassot (Valencia), Spain
[51]Institut für Hochenergiephysik, Österr. Akad. d. Wissensch., Nikolsdorfergasse 18, AT-1050 Vienna, Austria
[52]Inst. Nuclear Studies and University of Warsaw, Ul. Hoza 69, PL-00681 Warsaw, Poland
[53]Fachbereich Physik, University of Wuppertal, Postfach 100 127, DE-42097 Wuppertal, Germany

1 Introduction

During 1998, the DELPHI experiment at LEP accumulated an integrated luminosity of 158 pb^{-1} at a centre-of-mass energy, $\sqrt{s}$, of 188.7 GeV. Results of a search for neutralino pair production in these data are reported here. In a separate letter [1], these results are interpreted together with those of other DELPHI searches to set mass limits on neutralinos, sleptons and charginos.

In the Minimal Supersymmetric Standard Model (the MSSM) [2], there are four neutralinos $\tilde{\chi}^0_i, i = 1, 4$, numbered in order of increasing mass, and two charginos $\tilde{\chi}^\pm_j, j = 1, 2$. These are linear combinations of the supersymmetric (SUSY) partners of neutral and charged gauge and Higgs bosons. In the following, R-parity conservation is assumed, implying a stable lightest supersymmetric particle (LSP) which is assumed to be the $\tilde{\chi}^0_1$. R-parity conservation also implies pair-production of SUSY particles, each decaying (directly or indirectly) into a $\tilde{\chi}^0_1$, which is weakly interacting and escapes detection, giving a signature of missing energy and momentum.

The neutralinos can be pair-produced at LEP2 via s-channel Z exchange or t-channel exchange of a scalar electron (selectron, $\tilde{\mathrm{e}}$). The decay of heavier neutralino states to lighter ones typically involves emission of either a fermion-antifermion ($\mathrm{f\bar{f}}$) pair or a photon. If the scalar leptons (sleptons) are light, the two-body decay $\tilde{\chi}^0_i \to \ell\tilde{\ell}$ (followed by $\tilde{\ell} \to \tilde{\chi}^0_j \ell$) may dominate. Decays via charginos are also possible.

Of the detectable pair production channels (*i.e.* excluding $\tilde{\chi}^0_1\tilde{\chi}^0_1$), $\tilde{\chi}^0_1\tilde{\chi}^0_2$ and $\tilde{\chi}^0_1\tilde{\chi}^0_3$ are important for large regions in the parameter space. For a more complete coverage, however, one must also consider channels like $\tilde{\chi}^0_2\tilde{\chi}^0_3$ and $\tilde{\chi}^0_2\tilde{\chi}^0_4$, giving cascade decays with multiple jets or leptons in the final state.

Moreover, a light scalar tau lepton (stau, $\tilde{\tau}$) is likely to arise because of left-right mixing of the stau states. If the mass of the lighter stau, $M_{\tilde{\tau}_1}$, is close to $M_{\tilde{\chi}^0_1}$, the decay of the $\tilde{\tau}_1$ gives an undetectable neutralino and a low energy τ which is difficult to detect. In this case the search for chargino pair-production has a low efficiency since $\tilde{\chi}^\pm_1$ decays into $\tilde{\tau}_1\nu$, but the $\tilde{\chi}^0_1\tilde{\chi}^0_2$ and $\tilde{\chi}^0_2\tilde{\chi}^0_2$ channels are still detectable because of the τ produced directly in the decay $\tilde{\chi}^0_2 \to \tilde{\tau}_1\tau$. It is therefore important to search also for these channels [3].

In the search for $\tilde{\chi}^0_k\tilde{\chi}^0_1$ production with $\tilde{\chi}^0_k \to \tilde{\chi}^0_1 + \mathrm{f\bar{f}}$, the methods described in Refs. [4,5] were used, with minor changes. The signatures consist of pairs of jets or leptons with high missing energy and momentum and large acoplanarity [1]. In addition, several new searches were introduced in order to obtain a more complete coverage, in particular in the regions of low $M_{\tilde{\chi}^0_1}$:

- A search for multijet events, for example from $\tilde{\chi}^0_i\tilde{\chi}^0_j (i = 1, 2, j = 3, 4)$ with $\tilde{\chi}^0_j \to \tilde{\chi}^0_2 \mathrm{q\bar{q}}$ and $\tilde{\chi}^0_2$ decaying to $\tilde{\chi}^0_1 \mathrm{q\bar{q}}$ or $\tilde{\chi}^0_1\gamma$.
- A search for multilepton events for the corresponding decays to lepton pairs.
- A search for cascade decays with tau leptons, e.g. $\tilde{\chi}^0_2\tilde{\chi}^0_1$ production with $\tilde{\chi}^0_2 \to \tilde{\tau}\tau$ and $\tilde{\tau} \to \tilde{\chi}^0_1\tau$
- A search for events with low transverse energy and low multiplicity, e.g. arising from $\tilde{\chi}^0_2\tilde{\chi}^0_2$ production with $\tilde{\chi}^0_2 \to \tilde{\chi}^0_1\ell^+\ell^-$and low $M_{\tilde{\chi}^0_2} - M_{\tilde{\chi}^0_1}$, or from neutralino decays via intermediate slepton states.

The results showed no indication of a signal and were used to derive limits within the MSSM scheme with universal parameters at the high mass scale typical of Grand Unified Theories [2].

[1] This is defined as the the complement with respect to 180° of the angle between the jet- or lepton momenta projected on a plane transverse to the beam axis.

The DELPHI detector has been described elsewhere [6]. The central tracking system consists of a Time Projection Chamber (TPC) and a system of silicon tracking detectors and drift chambers. The electromagnetic calorimeters are symmetric around the plane perpendicular to the beam (θ=90°), with the High density Projection Chamber (HPC) in the barrel region ($\theta > 43°$) and the Forward Electromagnetic Calorimeter (FEMC) overlapping with the Small angle Tile Calorimeter (STIC) in the forward region ($1.7° < \theta < 35°$). The region of poor electromagnetic calorimetry at a polar angle close to 40° is instrumented by scintillators (hermeticity taggers) which serve to reject events with unmeasured photons.

2 Data samples and event generators

The total integrated luminosity collected by DELPHI during 1998 at $\sqrt{s} = 188.7$ GeV was 158 pb^{-1}, with 153 pb^{-1}of adequate data quality to be used in the present searches.

To evaluate the signal efficiencies and background contaminations, events were generated using several different programs. All relied on `JETSET` 7.4 [7], tuned to LEP 1 data [8], for quark fragmentation.

`SUSYGEN 2.2004` [9] was used to generate neutralino signal events and calculate cross-sections and branching ratios.

The background process $e^+e^- \to q\bar{q}(n\gamma)$ was generated with `PYTHIA 5.7` [7]. For $\mu^+\mu^-(\gamma)$ and $\tau^+\tau^-(\gamma)$, `DYMU3` [10] and `KORALZ 4.2` [11] were used, respectively, while the generator of Ref. [12] was used for $e^+e^- \to e^+e^-$ events. Four-fermion final states were generated using `EXCALIBUR` [13] and `grc4f` [14].

Two-photon interactions giving hadronic final states were generated using `TWOGAM` [15], and `PHOJET` [16], while for those giving leptonic final states the generator of Ref. [17] was used, including radiative corrections for $e^+e^-\mu^+\mu^-$ and $e^+e^-\tau^+\tau^-$ final states.

The generated signal and background events were passed through the detailed simulation of the DELPHI detector [6] and then processed with the same reconstruction and analysis programs as the real data. The numbers of simulated events from different background processes were several times the numbers in the real data, except for the number of simulated e^+e^- pairs from two-photon interactions which was only slightly larger than the number expected in the data.

In addition the simplified fast simulation program `SGV`, previously used in Ref. [18], was adopted. `SGV` takes into account inefficiencies and measurement errors in the different tracking detectors and calorimeters, as well as multiple scattering and the showering of electrons and photons in the tracking volume. This made it possible to estimate efficiencies for points in the MSSM parameter space without full simulation, and to take into account all contributing production and decay channels for a given point.

3 Event selection

The criteria for event selection described below were based on comparisons of simulated signal and background event samples. The different searches used were designed to be mutually exclusive, in order to allow easy combination of the results. All searches used the information from the hermeticity taggers to reject events with photons from initial state radiation lost in the otherwise insensitive region at polar angles around 40° and 140°. Events were rejected if there were active taggers in the direction of the missing momentum and not associated to reconstructed jets. Jets were reconstructed using the

LUCLUS algorithm [7] with $d_{\rm join} = 10$ GeV/c. Leptons were identified using the standard DELPHI "loose tag" criteria [6], except for electrons in the acoplanar leptons search (see section 3.2). There is a set of global event variables common to several searches. These were calculated based on the well-reconstructed particles in the event and include the total visible energy ($E_{\rm vis}$), the visible mass ($M_{\rm vis}$), total momentum transverse and longitudinal to the beam ($p_{\rm T}$,$p_{\rm L}$), and transverse energy ($E_{\rm T}$). The latter is defined as $\Sigma E_i \sin\theta_i$, where E_i and θ_i are the energy and polar angle of particle i. In several cases with two jets, their scaled acoplanarity (the acoplanarity multiplied by the sine of the smallest angle between a jet and the beam axis) was used.

3.1 Acoplanar jets search

Earlier variations of this search at lower energies have been described in Refs. [4,5].

At least five well reconstructed charged particles were required, including at least one with a transverse momentum with respect to the beam above 1.5 GeV/c. The sum of the moduli of momenta of well reconstructed charged particles had to be greater than 4 GeV/c, and the total transverse energy had to exceed 4 GeV. Two jets were required, each satisfying $10^\circ < \theta_{\rm jet} < 170^\circ$ and containing at least one well reconstructed charged particle. Tracks which were badly reconstructed, or did not originate from the interaction point, were required not to carry more energy than $0.45E_{\rm vis}$, where $E_{\rm vis}$ is the visible energy of well-reconstructed particles. This requirement typically removes events with a single badly reconstructed track with a very high momentum. In addition, the calorimeter energy associated to such tracks had to be less than $0.2E_{\rm vis}$ for an event to be accepted.

Several criteria were used to reject two-photon events: the fraction of the total energy carried by particles emitted within 30° of the beam had to be less than 60%, the polar angle of the total momentum had to satisfy $|\cos\theta_p| < 0.9$, and its transverse component had to exceed 6 GeV/c.

Figure 1(a) shows the distributions of invariant mass of the visible system ($M_{\rm vis}$) divided by $\sqrt{s}$, for real and simulated events passing the above selection. Here, and in the following, the simulated sample has been normalised to the integrated luminosity used for the data. As can be seen from the figure there is some excess of data events in the energy region corresponding to on-shell Z production with a lost photon from initial state radiation ("radiative return events"). This can be ascribed partly to a 3% deficit in the `PYTHIA` generator in this region as compared to analytical calculations [19], partly to four-fermion processes which were not taken into account completely, and partly to reconstruction problems in real events with jets in the forward direction. If such excess events in the data pass the later steps of the selection, the background is likely to be underestimated and the limits derived in the absence of a signal are thus conservative. In the final data sample the background from Z(γ) events is rather unimportant, however.

In the continued selection events were rejected if there was a neutral particle, either with an energy above 60 GeV, or isolated from the nearest jet by at least 20°, and with an energy above 20 GeV. These criteria served to remove radiative return events.

To reduce the WW background, events were rejected if they had a charged particle with momentum greater than 20 GeV/c or if the most isolated electron or muon (if any) had momentum greater than 10 GeV/c or was more than 20° from the nearest jet. Figure 1(c) shows the distributions of transverse momentum ($p_{\rm T}$) divided by $\sqrt{s}$ for real and simulated data, after the above selection.

In the last step of the selection, events were accepted if they satisfied any of the following three sets of criteria, optimised for different neutralino mass differences (ΔM).

The criteria involved the transverse momentum ($p_{\rm T}$), longitudinal momentum ($p_{\rm L}$), and invariant mass ($M_{\rm vis}$) of the visible system, as well as the mass recoiling against it ($M_{\rm rec}$). Also the acollinearity of the two jets and their scaled acoplanarity were used in this step. The events were accepted if:

(i) $M_{\rm vis} < 0.1\sqrt{s}/c^2$, $M_{\rm rec} > 0.7\sqrt{s}/c^2$, and $p_{\rm T} > 7$ GeV/c. In addition, the scaled acoplanarity was required to exceed 40°. These criteria are efficient for low ΔM ($\sim$10 GeV/c^2).

(ii) $0.1\sqrt{s}/c^2 < M_{\rm vis} < 0.3\sqrt{s}/c^2$, $M_{\rm rec} > 0.6\sqrt{s}/c^2$, and $p_{\rm T} > 8$ GeV/c. The scaled acoplanarity had to exceed 25°. These criteria are efficient for intermediate ΔM ($\sim$40 GeV/c^2).

(iii) $0.3\sqrt{s}/c^2 < M_{\rm vis} < 0.5\sqrt{s}/c^2$, $M_{\rm rec} > 0.45\sqrt{s}/c^2$, 12 GeV/$c < p_{\rm T} <$ 35 GeV/c, and $p_{\rm L} <$ 35 GeV/c. The scaled acoplanarity had to exceed 25°, and the acollinearity had to be below 55°. These criteria are efficient for high ΔM ($\sim$90 GeV/c^2).

Figure 1 (e) shows a comparison of the scaled acoplanarity for the real and simulated data events passing the last step of the selection.

3.2 Acoplanar leptons search

The search for acoplanar leptons selects events with exactly two isolated oppositely charged particles (lepton candidates) with momentum above 1 GeV/c, and at most five charged particles in total.

This search was slightly modified with respect to Ref. [4], as follows. The minimum number of TPC pad rows required for the two selected charged particles was increased from four to five. The lepton identification requirements were changed, accepting as electrons those particles which had an associated energy in the electromagnetic calorimeter exceeding half of the measured momentum, while for muons the "loose tag" criteria [6] were used. Either, both particles in the pair were required to be selected as electrons and not simultaneously identified as muons, or else both particles had to be muons. In addition to the acoplanarity, the acollinearity between the two particles also had to exceed 10°. The minimum transverse momentum required was increased from 5 to 6 GeV/c, and the maximum accepted energy in the STIC was reduced from 1 to 0.3 GeV. To improve the rejection of WW background, events with missing momentum above 45 GeV/c, and a scalar sum of the momenta of the two selected particles in excess of 100 GeV/c, were rejected. Prior to the last step of the selection 65 real data events were accepted, while the expected background was 62.8±4.4 events, with a contribution of 31.1±0.6 events from $\rm W^+W^-$ production. As in Ref. [4], the last step involved three sets of criteria sensitive to different ΔM ranges. These criteria were unchanged, except for the minimal missing mass required in the selection optimised for large ΔM, which was changed from $0.4\sqrt{s}/c^2$ to $0.2\sqrt{s}/c^2$.

Figure 1 (b,d,f) shows a comparison between real and simulated data for events passing the initial step of the above selection corresponding to rejection of Bhabha events (b), passing the intermediate step corresponding to rejection of two-photon events (d), and passing the last step (f). Real and simulated data were in good agreement throughout.

3.3 Multijet search

The multijet search was optimised for cascade decays of neutralinos with large mass splittings, giving high energy jets. Events with energetic photons, characteristic of the

decay $\tilde{\chi}_2^0 \to \tilde{\chi}_1^0\gamma$, were subjected to less stringent selection criteria, giving a separate set of selected events with low background and comparatively high efficiency.

At least five well-reconstructed charged particles were required, and at least one of these had to have a transverse momentum exceeding 2.5 GeV/c. The transverse energy of the event had to be greater than 25 GeV, and the total energy of tracks which were badly reconstructed or did not originate from the interaction point was required to be less than 30 GeV and less than 45% of the visible energy. In addition, the calorimeter energy associated to such tracks had to be less than 20% of $E_{\rm vis}$. Figure 2 (a) shows the distributions of $M_{\rm vis}$ divided by the centre-of-mass energy for real data and simulated background events passing the above selection. The excess of "radiative return" events observed in the acoplanar jets search is visible also here, and the comments of section 3.1 apply. Similarly, the deficit of events in the real data with $M_{\rm vis}/\sqrt{s}$ close to unity can be partly explained by a known excess of PYTHIA events with little initial state radiation.

The total energy in the electromagnetic calorimeters had to be less than 70 GeV, and there had to be no single calorimeter shower above 60 GeV. The energy carried by particles within 30° of the beam had to be less than 60% of the visible energy. The total visible energy had to be less than 135 GeV, the polar angle of the total momentum had to satisfy $|\cos\theta_p| < 0.9$, and the transverse momentum had to exceed 6 GeV/c. Figure 2 (c) gives a comparison of the $p_{\rm T}/\sqrt{s}$-distributions for real data and simulated background following the above selection.

The scaled acoplanarity (see section 3.1), calculated forcing the number of jets to two, had to be greater than 10°. The polar angle of the most energetic jet had to be outside the range between 85° and 95° to avoid an insensitive detector region close to 90°, and its energy had to be less than 56 GeV.

To reject WW background it was required that there be no charged particle with a momentum above 30 GeV/c, and that the momentum of the most isolated electron or muon (if any) be below 10 GeV/c, or below 4 GeV/c if the angle between the lepton and the nearest jet was greater than 20°.

Events with a photon signature were then selected on the basis of reconstructed photons in the polar angle range between 20° and 160°, isolated by more than 20° from the nearest charged particle track. If there was only one such photon its energy was required to be between 10 GeV and 40 GeV; with more than one photon, at least two had to have energy greater than 10 GeV.

For the complementary sample, without a photon signature, two additional requirements were imposed to reject Zγ events: the mass recoiling against the system of visible particles had to be greater than 100 GeV/c^2, and all jets with energy above 20 GeV had to have a ratio of energy in charged particles to energy in neutral particles which was above 0.15.

Lastly, events selected by the searches for acoplanar jets or leptons (sections 3.1 and 3.2) were rejected. Figure 2 (e) shows the acoplanarity distributions for real and simulated events without a photon signature passing the last step of the selection.

3.4 Multilepton search

The multilepton search is sensitive to cascade decays involving leptons, which can dominate if there are light sleptons.

The first step in the selection, in common with the tau cascade and low E_T searches (sections 3.5 and 3.6), was as follows. The number of charged particles was required to be at least two and at most eight, and events with more than four neutral particles were

rejected. The reconstructed invariant mass had to be below 120 GeV/c^2, and the recoil mass above 20 GeV/c^2. The calorimeter energy associated to particles which were badly reconstructed or did not originate at the vertex, $E_{\rm bc}$, was required not to exceed 0.4 $E_{\rm vis}$, while the energy of well reconstructed charged particles had to be greater than 0.2 $E_{\rm vis}$. It was also required that $E_{\rm vis}+E_{\rm bc}<140$ GeV.

In the following step, at least two charged particles were required to be identified leptons. Figure 2 (b) shows a comparison between $M_{\rm vis}/\sqrt{s}$ distributions for real and simulated events passing the above selection.

To reject Zγ, two-photon, and Bhabha events, the transverse momentum of the event was required to exceeded 8 GeV/c, and the polar angle of the total momentum to satisfy $|\cos\theta_p| < 0.9$. The transverse energy of the event had to be greater than 25 GeV, and the energy in the STIC was required to be less than 10 GeV. The distributions of $p_{\rm T}/\sqrt{s}$ for real and simulated data, following the above selection, are compared in figure 2 (d).

For events with exactly two isolated well-reconstructed charged particles the following requirements were imposed. The acoplanarity and acollinearity of these two particles had to exceed 15° and 6°, respectively. If the total energy in electromagnetic calorimeters exceeded 50 GeV the acollinearity was required to be greater than 10°. To reject W pairs decaying leptonically it was required that the product of charge and cosine of polar angle was less than -0.1 for each of the two charged particles.

For events with two reconstructed jets, the scaled acoplanarity was required to be greater than 15°.

Lastly, events selected by the searches for acoplanar jets or leptons (sections 3.1 and 3.2), or by the multijet search (section 3.3), were rejected. Figure 2 (f) shows the distributions of acoplanarity for real and simulated data, following the above selection.

3.5 Tau cascade search

The tau cascade search is sensitive to $\tilde{\chi}^0_1\tilde{\chi}^0_2$ production with $\tilde{\chi}^0_2 \to \tilde{\tau}\tau$ and $\tilde{\tau} \to \tilde{\chi}^0_1\tau$, where the second τ produced has very low energy. The first step of the selection was the same as for the multilepton search (section 3.4), with the additional requirement of no more than two reconstructed jets. Two or more of the charged particles also had to satisfy stricter criteria on reconstruction and impact parameters.

In the next step, the highest and second highest momenta of charged particles were required to be below 50 GeV/c and 25 GeV/c, respectively, and at least one charged particle had to have a transverse momentum above 2.5 GeV/c. Events with neutral showers above 300 MeV within 20° of the beam axis were rejected. The visible mass distributions, for real and simulated data at this stage of the selection, are compared in figure 3 (a).

The criteria to reject Zγ, two-photon, and Bhabha events, were the same as for the multilepton search (section 3.4), except for the minimum transverse momentum which was reduced to 7 GeV/c, and the removal of the transverse energy requirement.

Figure 3 (c) shows distributions of $E_{\rm vis}/\sqrt{s}$ as a comparison between real and simulated data, selected with the above criteria. There is an evident excess in the energy region dominated by two-photon interactions. This has been studied in a recent workshop on generators at LEP2 [20]. The background from two-photon interactions giving hadronic final states is known to be underestimated, and the process $\gamma\gamma \to \ell^+\ell^-$ is also not well described by simulation. In the case of $\tau^+\tau^-$ the treatment of tau decays in the generator was approximate, and polarisation effects were absent. Furthermore, some four-fermion processes were not completely accounted for in the simulation. If the two-

photon background the end of the selection is also underestimated the obtained limits are conservative, but in any case this background is not the dominant one.

Events with exactly two isolated, well-reconstructed, oppositely charged particles were required to have acollinearity and acoplanarity above 60°. The smaller of the two momenta had to be below 70% of the greater one, and below 10 GeV/c.

For events with two reconstructed jets the scaled acoplanarity (see section 3.1) was required to be greater than 20°, and the acoplanarity and the acollinearity greater than 60°.

Lastly, events selected by the searches for acoplanar leptons or jets (sections 3.2 and 3.1) or the multilepton search (section 3.4) were rejected. Figure 3 (e) shows the acoplanarity distribution for events passing the complete selection, in real data and simulated background.

3.6 Low transverse energy search

The low transverse energy (E_{T}) search was designed to complement the multilepton search for cascade decays or $\tilde{\chi}^0_2\tilde{\chi}^0_2$ production with low mass splitting where $\tilde{\chi}^0_2 \to \tilde{\chi}^0_1\ell^+\ell^-$. The first step of the selection was the same as for the multilepton search. In the second step, it was required that there be at least three and at most five charged particles, and that all had momenta above 500 MeV/c. Two or more of the charged particles had to satisfy stricter criteria on reconstruction and impact parameters.

In the third step, the highest and second highest momenta of charged particles were required to be below 50 and 25 GeV/c, respectively. At least one charged particle had to have a transverse momentum above 2.5 GeV/c, and at least one had to be an identified lepton. There had to be no neutral shower within 20° of the beam axis, and the second highest jet energy had to be below 30 GeV.

Figure 3 (b) shows the distributions of $p_{\mathrm{T}}/\sqrt{s}$ for events fulfilling the above criteria in the real and simulated data. Excess data events from two-photon interactions and the "radiative return" process are visible here too. Again, this could give too conservative limits if such excess events were to survive the complete selection. The overall effect of the low transverse energy search on the obtained limits is rather small, however.

The bulk of the two-photon background was rejected by the requirements that the polar angle of the total momentum had to satisfy $|\cos\theta_p| < 0.9$, and that the transverse energy of the event had to be greater than 4 GeV. The distributions of $M_{\mathrm{vis}}/\sqrt{s}$ for the real and simulated data, following these requirements, are compared in figure 3 (d).

The specific requirements for events with exactly two well reconstructed, isolated, charged particles were the same as in section 3.4, with the additional requirement that at least one of the tracks had to have a momentum below 15 GeV/c.

Events with transverse momentum exceeding 8 GeV/c and transverse energy greater than 10 GeV were rejected, unless the scaled acoplanarity, calculated forcing the number of jets to two, was above 20°.

Lastly, events selected by the searches for acoplanar jets or leptons (sections 3.1 and 3.2), the multilepton search (section 3.4), or the tau cascade search (section 3.5) were rejected. Figure 3 (f) shows the distributions of scaled acoplanarity for real and simulated events passing the complete selection.

4 Selected events and expected backgrounds

Table 1 shows the number of events selected in the different searches in real data and the numbers expected from the Standard Model background. Also shown are the main background sources contributing in each channel and the typical efficiency of each search for MSSM points where it is relevant.

Search	Data	Total bkg.	Main bkg.	Typical eff. (%)
Acoplanar jets	19	21.0±1.6	W^+W^-,ZZ	10 – 30
Acoplanar electrons	16	20.7±3.7	W^+W^-,$\gamma\gamma$	10 – 40
Acoplanar muons	16	14.6±1.3	W^+W^-,$\gamma\gamma$	10 – 40
Multijets, γ:s	2	4.3±0.5	Zγ	10 – 20
Multijets, no γ:s	39	31.8±1.9	Zγ, W^+W^-	10 – 40
Multileptons	23	28.2±1.2	W^+W^-	30 – 50
Tau cascades	8	9.0±1.0	W^+W^-,$\gamma\gamma(\rightarrow \mu^+\mu^-)$	13 – 19
Low E_{T}	18	19.0±3.3	$\gamma\gamma(\rightarrow \tau^+\tau^-)$	7 – 10

Table 1: Results of the different searches. The typical efficiency of each search for MSSM points where it is relevant is shown. The efficiencies depend typically on the masses of the sparticles involved in the process. For any given search, events are explicitly rejected if accepted by one of the searches appearing earlier in the table.

The main reason for the variation of the efficiencies is the variation of the masses of the particles involved in the process. The explicit rejection of events to avoid overlapping selections limits the efficiencies for those searches in which such rejection is performed (see section 3 and table 1). The total number of events selected in the different searches was 141, with 149±6 background events expected. The errors given for the background estimates are due to the finite sizes of the simulated background samples. No error was assigned to account for the excesses of data events seen at early stages of the selections. In conclusion, the results are in good agreement with the expectation from Standard Model background, and no indication of a signal was found.

5 Signal efficiencies and upper limits

In the absence of a signal, cross-section limits were derived based on the efficiencies for simulated neutralino events. A total of 360 000 $\tilde{\chi}^0_1\tilde{\chi}^0_2$ events was simulated for 108 different combinations of masses with $M_{\tilde{\chi}^0_1}$ and $M_{\tilde{\chi}^0_2}$ ranging from 5 GeV/c^2 to 90 GeV/c^2 and from 20 GeV/c^2 to 180 GeV/c^2, respectively, and for different $\tilde{\chi}^0_2$ decay modes ($\mathrm{q\bar{q}}\tilde{\chi}^0_1$, $\mu^+\mu^-\tilde{\chi}^0_1$, $\mathrm{e^+e^-}\tilde{\chi}^0_1$, $\tilde{\tau}\tau$). A further 100 000 $\tilde{\chi}^0_2\tilde{\chi}^0_{3,4}$ events with cascade decays, were simulated for 56 different points. In addition, about $5{\cdot}10^8$ events were simulated using `SGV` in order to obtain signal efficiencies for about 10^5 MSSM points.

Figures 4 and 5 show the expected distributions for some relevant event variables for $\tilde{\chi}^0_1\tilde{\chi}^0_2$ production as obtained using the full detector simulation and `SGV`. The efficiencies obtained using SGV agreed typically to ±10% relative with those obtained by full simulation. Figure 6 shows a comparison between `SGV` efficiencies (curves) and those from the full simulation (points) as a function of ΔM in the topologies with acoplanar leptons and acoplanar jets. In the case of leptonic events the SGV efficiencies are generally lower, giving conservative limits. In the hadronic case the SGV efficiencies tend to be higher, and they were therefore conservatively reduced by 20% in the limit calculations. The effect on the $M_{\tilde{\chi}^0_1}$ limit for $\tan\beta = 1$ [1] was found to be completely negligible.

The limits for the $\tilde{\chi}^0_1\tilde{\chi}^0_2$ production, as obtained from the searches for acoplanar leptons and jets, are shown in Figs. 7 assuming different branching ratios. Similarly, Figs. 8(a,b) show cross-section limits for $\tilde{\chi}^0_2\tilde{\chi}^0_i$ production ($i = 3$ or 4). For each mass combination, the limits were obtained by examining many possible (μ,M_2) points for several $\tan\beta$ values and high m_0, where $\tilde{\chi}^0_2\tilde{\chi}^0_i$ production was kinematically allowed. The point giving the worst limit was taken. In the white regions marked "Not allowed", no such points were found. Figure 8(a) shows the limit obtained using a Bayesian combination [21] of the results from the multijet and acoplanar jet searches in the case where $\tilde{\chi}^0_i \to \tilde{\chi}^0_2 q\bar{q}$ and $\tilde{\chi}^0_2 \to \tilde{\chi}^0_1 q\bar{q}$. Figure 8(b) gives the corresponding limits when $\tilde{\chi}^0_2 \to \tilde{\chi}^0_1\gamma$, as obtained from the search for multijet events with a photon signature.

In addition to such limits on the production cross-sections, the approach using a fast simulation makes it possible to scan regions of the MSSM parameter space and calculate the efficiencies directly at each point, simulating all neutralino production channels and decay chains. Since they were defined to be mutually exclusive, the different selections can be combined using the Bayesian multi-channel approach [21] to obtain the exclusion confidence level for each set of MSSM parameters[2]. Figs. 9 and 10 show the regions excluded by the different contributing searches in the (μ,M_2) plane for $\tan\beta = 1$ and $m_0 = 1\,\mathrm{TeV}/c^2$ and $80\ \mathrm{GeV}/c^2$, respectively. Also shown are the combined exclusion regions for the two values of m_0. In the region indicated as "Not allowed" the lightest chargino is lighter than $\tilde{\chi}^0_1$. Although the process for which it was designed is not important here, the τ cascade search is efficient for cascade decays involving leptons in the region close to $\mu = 0$ for $m_0 = 80\,\mathrm{GeV}/c^2$, and when the chargino-neutralino mass difference is small. (In the latter case the decay $\tilde{\chi}^0_{2,3} \to \tilde{\chi}^\pm_1 \ell\nu$ is followed by an almost invisible chargino decay.)

The thin dotted curve in the figures indicates the chargino isomass contour corresponding to the kinematic limit for $\tilde{\chi}^+_1\tilde{\chi}^-_1$ production. For high m_0 this is very close to the exclusion limit from chargino searches. For low m_0 the region excluded from chargino production is smaller [1], but the neutralino excluded region is increased, as can be seen from Figure 10. Therefore the overall limit on $M_{\tilde{\chi}^0_1}$ for $\tan\beta = 1$ is determined by the intersection of the chargino isomass contour with the region excluded by neutralinos for high m_0 [1]. The corresponding $\tilde{\chi}^0_1$ isomass contour is shown as the thin dashed curve.

At low m_0 and low M_2, the region excluded by neutralinos shrinks with increasing $\tan\beta$ due to enhancement of the invisible $\tilde{\chi}^0_2 \to \tilde{\nu}\nu$, $\tilde{\nu} \to \nu\tilde{\chi}^0_1$ decay channel. There is no substantial change of the high m_0 exclusion region with the increase of $\tan\beta$.

6 Summary

Searches for neutralinos at $\sqrt{s} = 188.7$ GeV, using several mutually exclusive sets of criteria, gave no indications of a signal. As a consequence, upper limits on cross-sections for different topologies were derived, ranging from about 0.1 pb to several picobarn. The efficiencies computed with a full simulation of the DELPHI detector were extended to the whole range of the SUSY parameters explored by using a fast detector simulation, which included all neutralino production and decay channels. Exclusion regions in the MSSM parameter space were then derived. The methods used were designed for deriving general MSSM mass limits in the Minimal Supersymmetric Standard Model, as done in a separate letter [1].

[2]The same procedure is applied in Ref. [1], including also the production of other supersymmetric particles.

Acknowledgements

We are greatly indebted to our technical collaborators, to the members of the CERN-SL Division for the excellent performance of the LEP collider, and to the funding agencies for their support in building and operating the DELPHI detector. We acknowledge in particular the support of the Austrian Federal Ministry of Science and Traffics, GZ 616.364/2-III/2a/98, FNRS–FWO, Belgium, FINEP, CNPq, CAPES, FUJB and FAPERJ, Brazil, Czech Ministry of Industry and Trade, GA CR 202/96/0450 and GA AVCR A1010521, Danish Natural Research Council, Commission of the European Communities (DG XII), Direction des Sciences de la Matière, CEA, France, Bundesministerium für Bildung, Wissenschaft, Forschung und Technologie, Germany, General Secretariat for Research and Technology, Greece, National Science Foundation (NWO) and Foundation for Research on Matter (FOM), The Netherlands, Norwegian Research Council, State Committee for Scientific Research, Poland, 2P03B06015, 2P03B03311 and SPUB/P03/178/98, JNICT–Junta Nacional de Investigação Científica e Tecnológica, Portugal, Vedecka grantova agentura MS SR, Slovakia, Nr. 95/5195/134, Ministry of Science and Technology of the Republic of Slovenia, CICYT, Spain, AEN96–1661 and AEN96-1681, The Swedish Natural Science Research Council, Particle Physics and Astronomy Research Council, UK, Department of Energy, USA, DE–FG02–94ER40817.

References

[1] DELPHI Coll., P. Abreu *et al.*, Phys. Lett. **B489** (2000) 38.

[2] P. Fayet and S. Ferrara, Phys. Rep. **32** (1977) 249;
H.P. Nilles, Phys. Rep. **110** (1984) 1;
H.E. Haber and G.L. Kane, Phys. Rep. **117** (1985) 75.

[3] LEP SUSY Working Group, ALEPH, DELPHI, L3 and OPAL experiments, note LEPSUSYWG/99-03. See `http://lepsusy.web.cern.ch/lepsusy/`.

[4] DELPHI Coll., P. Abreu *et al.*, Phys. Lett. **B446** (1999) 75.

[5] DELPHI Coll., P. Abreu *et al.*, E. Phys. J. **C1** (1998) 1.

[6] DELPHI Coll., P. Aarnio *et al.*, Nucl. Instr. and Meth. **A303** (1991) 233;
DELPHI Coll., P. Abreu *et al.*, Nucl. Instr. and Meth. **A378** (1996) 57.

[7] T. Sjöstrand, Comp. Phys. Comm. **39** (1986) 347;
T. Sjöstrand, `PYTHIA 5.6` *and* `JETSET 7.3`, CERN-TH/6488-92.

[8] DELPHI Coll., P. Abreu *et al.*, Z. Phys. **C73** (1996) 11.

[9] S. Katsanevas and P. Morawitz, Comp. Phys. Comm. **112** (1998) 227.

[10] J.E. Campagne and R. Zitoun, Z. Phys. **C43** (1989) 469.

[11] S. Jadach and Z. Was, Comp. Phys. Comm. **79** (1994) 503.

[12] F.A. Berends, R. Kleiss, W. Hollik, Nucl. Phys. **B304** (1988) 712.

[13] F.A. Berends, R. Pittau, R. Kleiss, Comp. Phys. Comm. **85** (1995) 437.

[14] J. Fujimoto *et al.*, Comp. Phys. Comm. **100** (1997) 128.

[15] S. Nova, A. Olshevski, and T. Todorov, in CERN Report 96-01, Vol. 2, p.224.

[16] R. Engel, Z. Phys. **C66** (1995) 203;
R. Engel and J. Ranft, Phys. Rev. **D54** (1996) 4244.

[17] F.A. Berends, P.H. Daverveldt, R. Kleiss, Comp. Phys. Comm. **40** (1986) 271, Comp. Phys. Comm. **40** (1986) 285, Comp. Phys. Comm. **40** (1986) 309.

[18] DELPHI Coll., P. Abreu *et al.*, E. Phys. J. **C6** (1999) 385.

[19] D. Bardin *et al.*, "ZFITTER v.6.21: A Semi-Analytical Program for Fermion Pair Production in e^+e^- Annihilation.", DESY 99-070, hep-ph/9908433, submitted to Comp. Phys. Comm.

[20] T.Alderweireld *et al.*, in "Reports of the working groups on precision calculations for LEP2 Physics", CERN 2000-009.

[21] V.F. Obraztsov, Nucl. Instr. and Meth. **A316** (1992) 388,
erratum, *ibid.* **A399** (1997) 500.

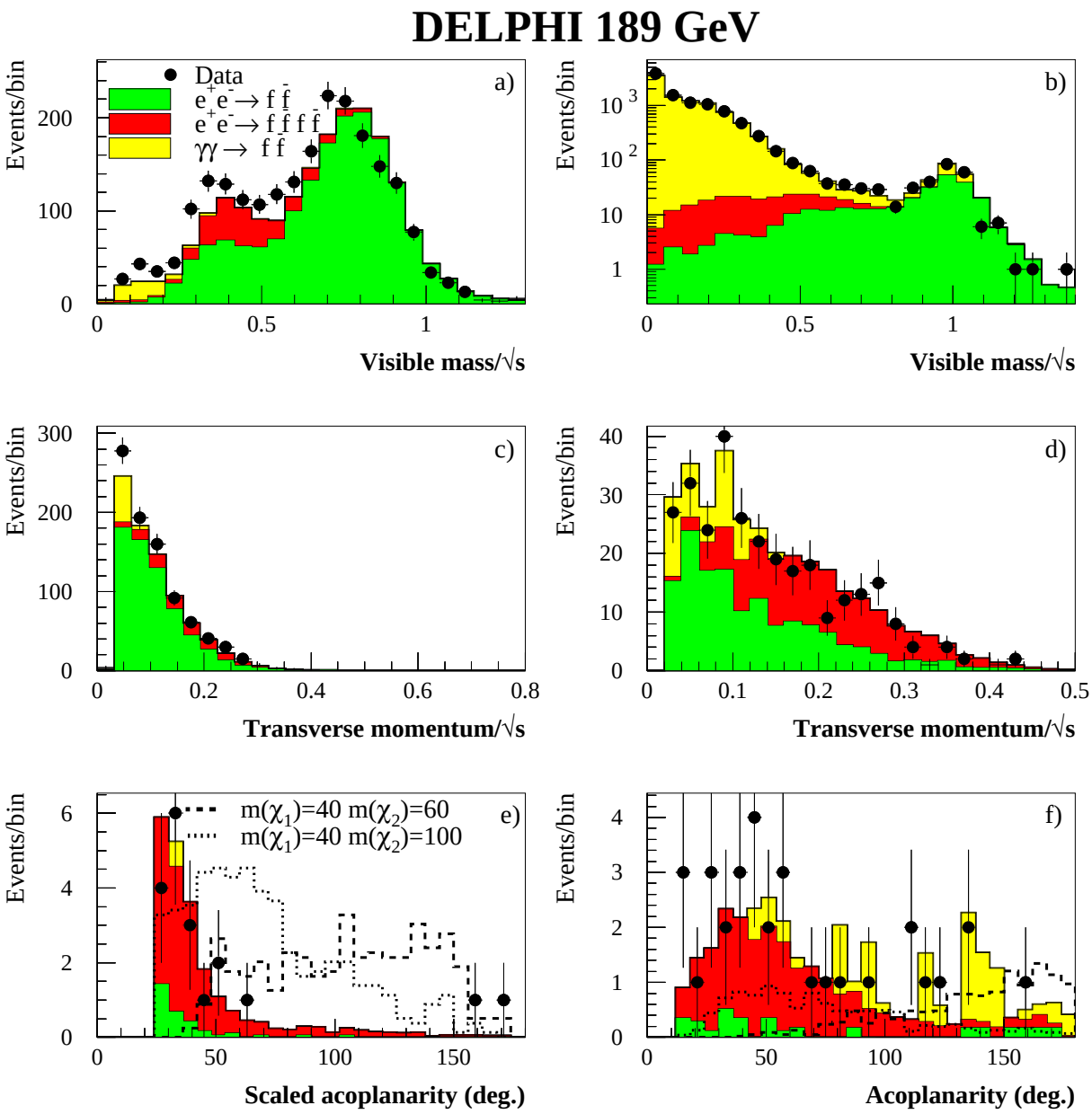

Figure 1: The comparison between the real and simulated data for the acoplanar jet selection (a,c,e) and acoplanar lepton selection (b,d,f) is shown. Plots (a,b) show the visible mass divided by the centre-of-mass energy at an initial stage of the selections. Plots (c,e) shows the missing transverse momentum divided by centre-of-mass energy at an intermediate stage of the selections. Plots (e,f) show acoplanarity distributions after the last step of the selections. The selections are described in sections 3.1 and 3.2. Plots (e,f) also show the expected signal of $\tilde{\chi}_1^0\tilde{\chi}_2^0$ production for two different neutralino mass combinations assuming a cross-section of 1 pb and the decay $\tilde{\chi}_2^0 \to Z^*\tilde{\chi}_1^0$.

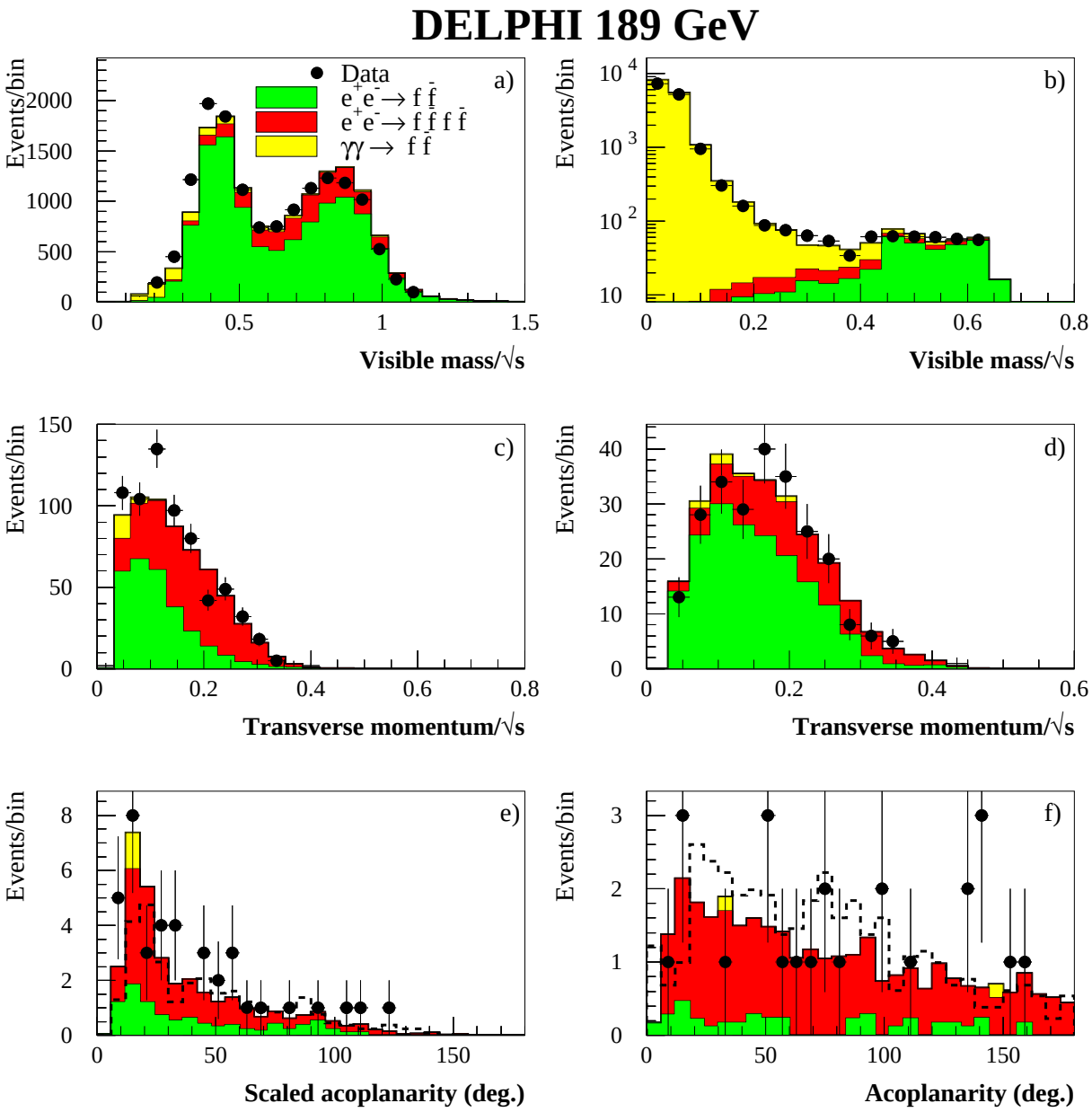

Figure 2: The comparison between the real and simulated data for the multijet selection (a,c,e) and multilepton selection (b,d,f) is shown at three different stages of the selection. Plots (a,b) show the $M_{\rm vis}$ divided by the centre-of-mass energy at an initial stage of the selections. Plots (c,d) show the missing transverse momentum at an intermediate stage of the selections. Plots (e,f) show the acoplanarity after the last step of the selections. The selections are described in sections 3.3 and 3.4. The distributions expected for $\tilde{\chi}^0_2\tilde{\chi}^0_3$ production with $\tilde{\chi}^0_3 \to \tilde{\chi}^0_2 f\bar{f} \to \tilde{\chi}^0_1 f'\bar{f}'$, normalised to a cross-section of 2 pb, are also shown for decays into quark and lepton pairs in e) and f), respectively (dashed histograms). Equal mass differences $M_{\tilde{\chi}^0_3} - M_{\tilde{\chi}^0_2} = M_{\tilde{\chi}^0_2} - M_{\tilde{\chi}^0_1} = 25$ GeV/c^2 were assumed.

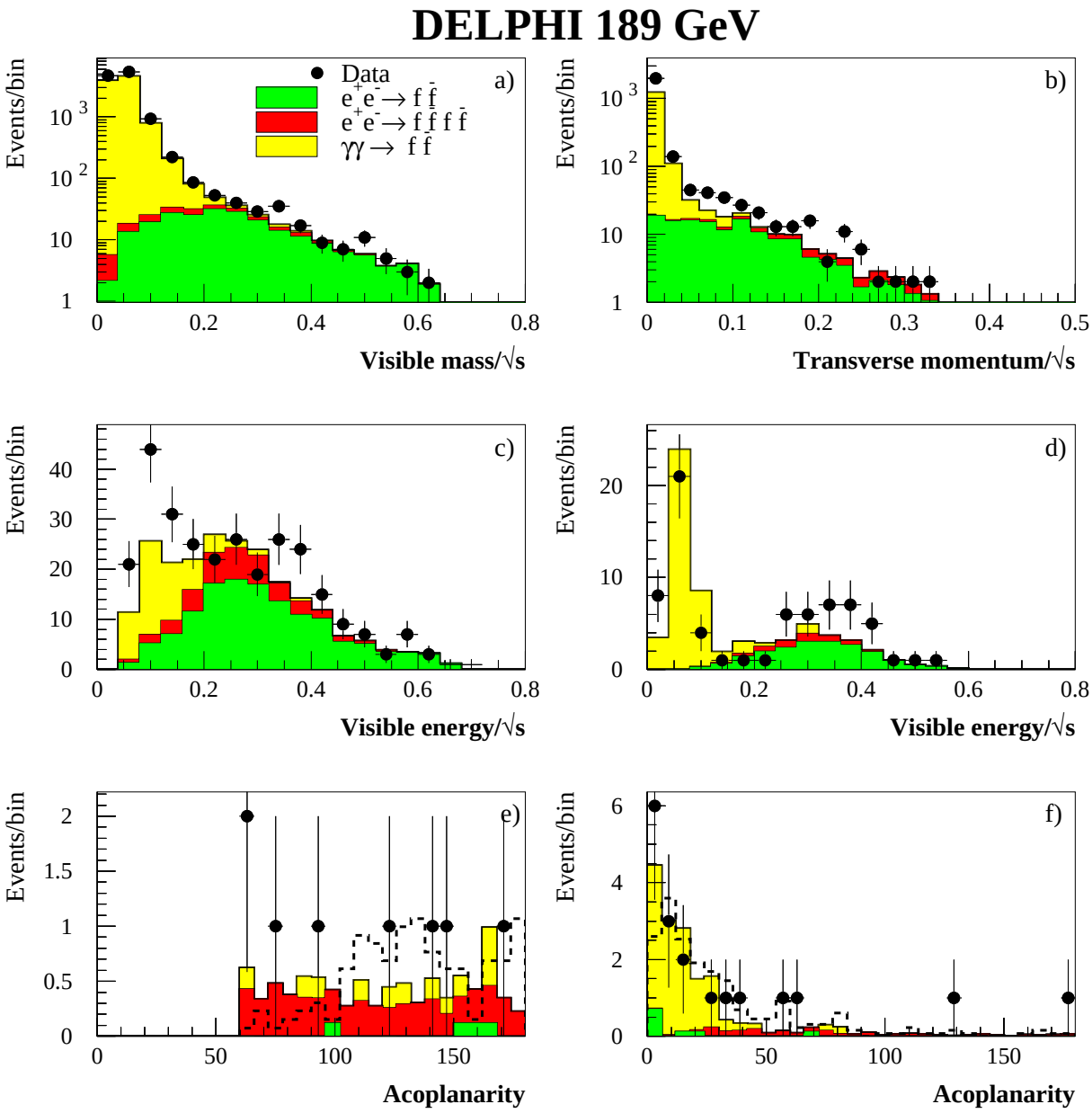

Figure 3: The comparison between the real and simulated data for the tau cascade selection (a,c,e) and low E_{T} selection (b,d,f) is shown. Plots (a,b) show the M_{vis} divided by the centre-of-mass energy and transverse momentum divided by the centre-of-mass energy at an initial stage of the selections. Plots (c,d) show the visible energy divided by the centre-of-mass energy at an intermediate stage of the selections. Plots (e,f) show the acoplanarity after the last step of the selections. The selections are described in sections 3.5 and 3.6. The dashed line in e) shows the tau cascade signal expected from $\tilde{\chi}^0_1\tilde{\chi}^0_2$ production with $\tilde{\chi}^0_2 \to \tau\tilde{\tau} \to \tau\tau\tilde{\chi}^0_1$, $M_{\tilde{\chi}^0_1} = 34.8$ GeV/c^2, $M_{\tilde{\tau}} = 36.8$ GeV/c^2, and $M_{\tilde{\chi}^0_2} = 60$ GeV/c^2. In f) the dashed line corresponds to $\tilde{\chi}^0_2\tilde{\chi}^0_2$ production with $\tilde{\chi}^0_2 \to \tilde{\chi}^0_1\ell^+\ell^-(\ell = \mathrm{e},\mu,\tau)$, $M_{\tilde{\chi}^0_1} = 35$ GeV/c^2, and $M_{\tilde{\chi}^0_2} = 40$ GeV/c^2. The signals are normalised to 2 pb.

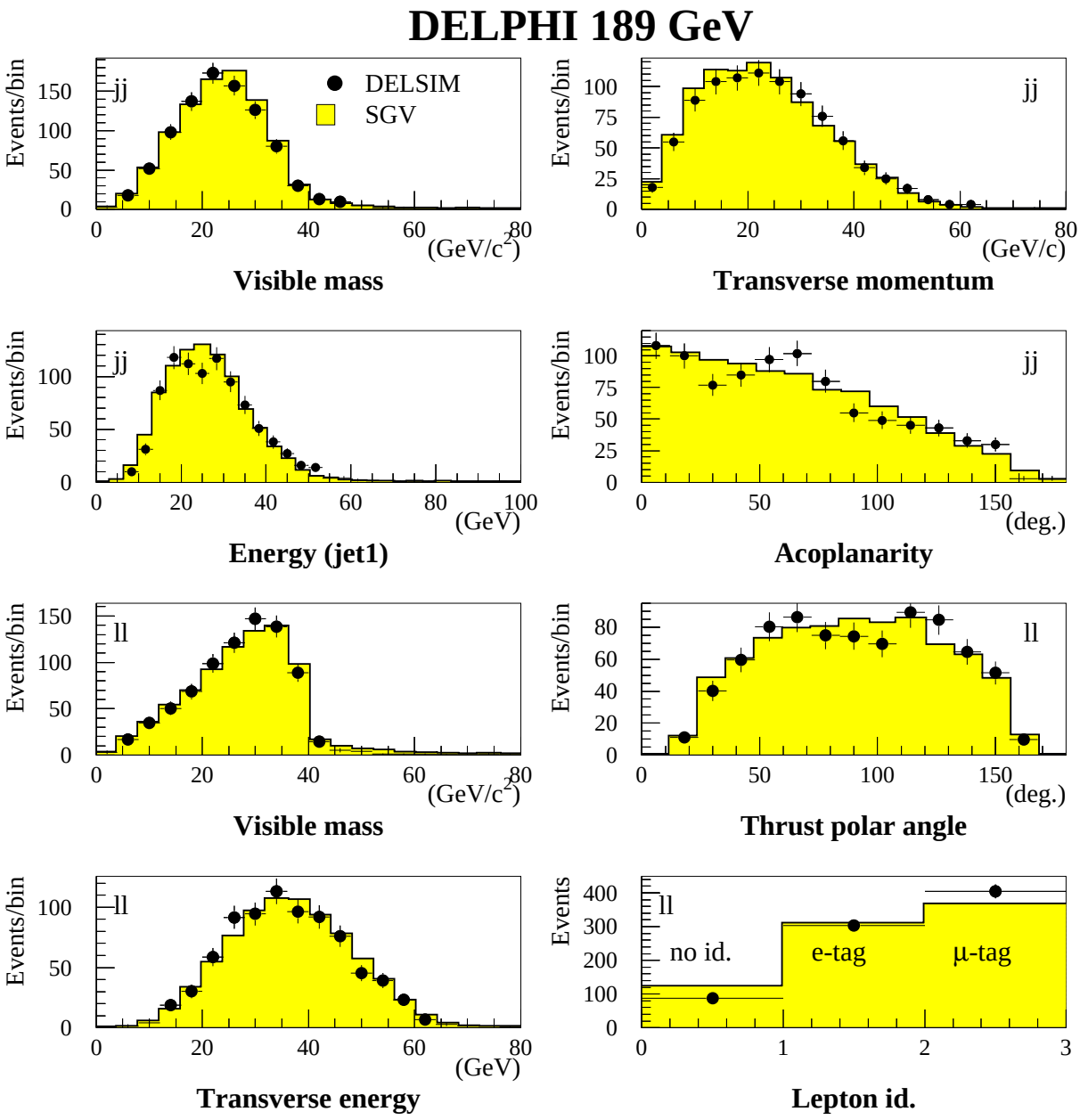

Figure 4: The expected distributions of relevant event variables characterizing the $\tilde{\chi}_1^0\tilde{\chi}_2^0$ production with $M_{\tilde{\chi}_1^0} = 40$ GeV/c^2 and $M_{\tilde{\chi}_2^0} = 80$ GeV/c^2, as obtained using the full detector simulation (`DELSIM`) and `SGV` for the acoplanar jet (jj) topology (upper four plots) and acoplanar lepton (ll) topology (lower four plots). The decays $\tilde{\chi}_2^0 \to \tilde{\chi}_1^0 q\bar{q}$ or $\tilde{\chi}_1^0 \ell^+\ell^-$ were assumed as appropriate ($\ell^+\ell^-$ denotes e^+e^- and $\mu^+\mu^-$ in equal proportions).

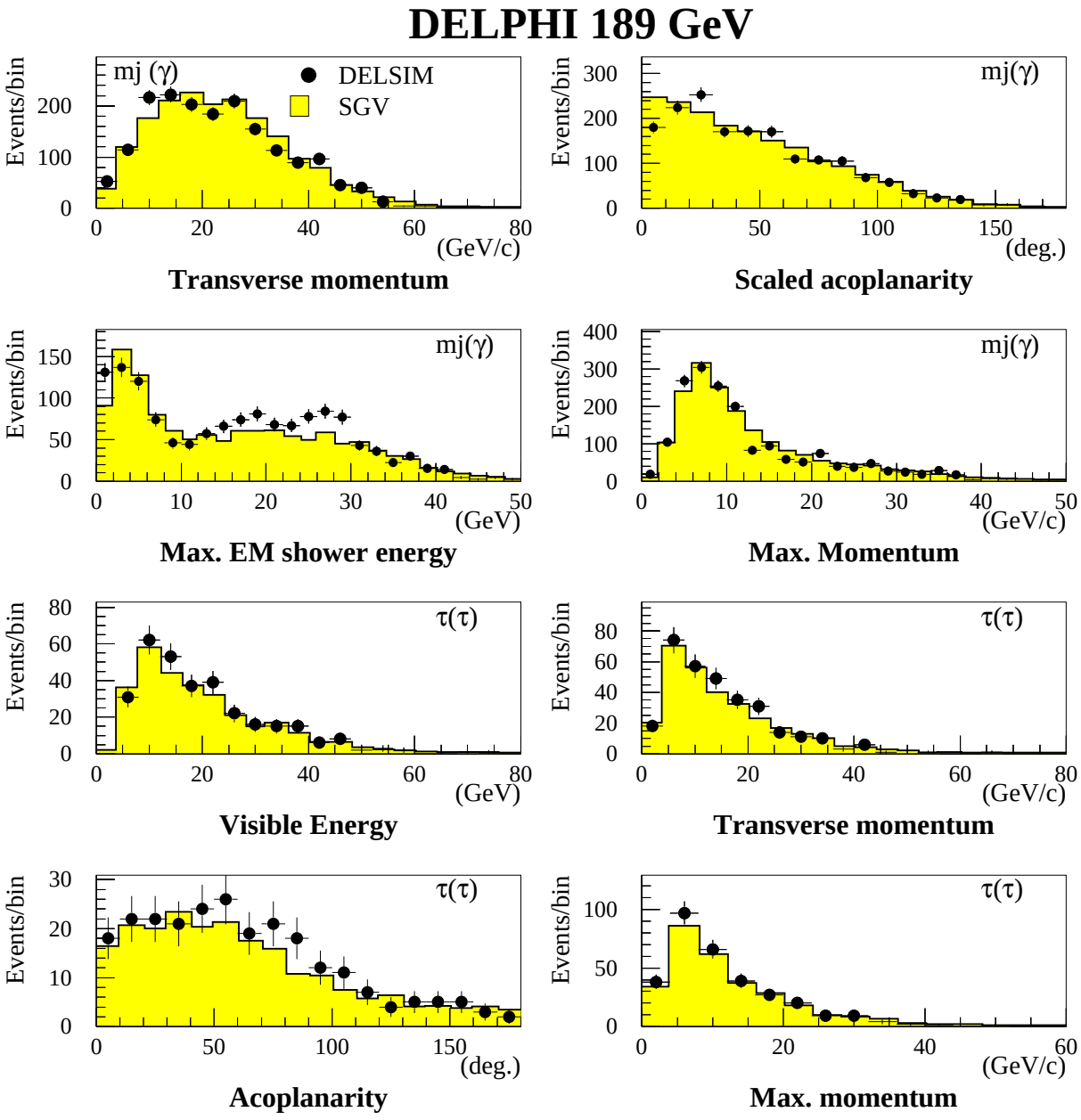

Figure 5: The expected distributions of relevant event variables characterizing neutralino production for the multijet topologies (upper four plots) and the tau cascade topology (lower four plots). In the multijet case chosen, $\tilde{\chi}_4^0\tilde{\chi}_2^0$ production dominates with 50% of the $\tilde{\chi}_2^0$ decaying to $\tilde{\chi}_1^0\gamma$. The neutralino masses are $M_{\tilde{\chi}_1^0} = 31$ GeV/c^2, $M_{\tilde{\chi}_2^0} = 60$ GeV/c^2, and $M_{\tilde{\chi}_4^0} = 100$ GeV/c^2. In the tau cascade case, $\tilde{\chi}_1^0\tilde{\chi}_2^0$ production with $\tilde{\chi}_2^0 \to \tau\tilde{\tau} \to \tau\tau\tilde{\chi}_1^0$ was assumed with $M_{\tilde{\chi}_1^0} = 34.8$ GeV/c^2, $M_{\tilde{\tau}} = 36.8$ GeV/c^2, and $M_{\tilde{\chi}_2^0} = 60$ GeV/c^2.

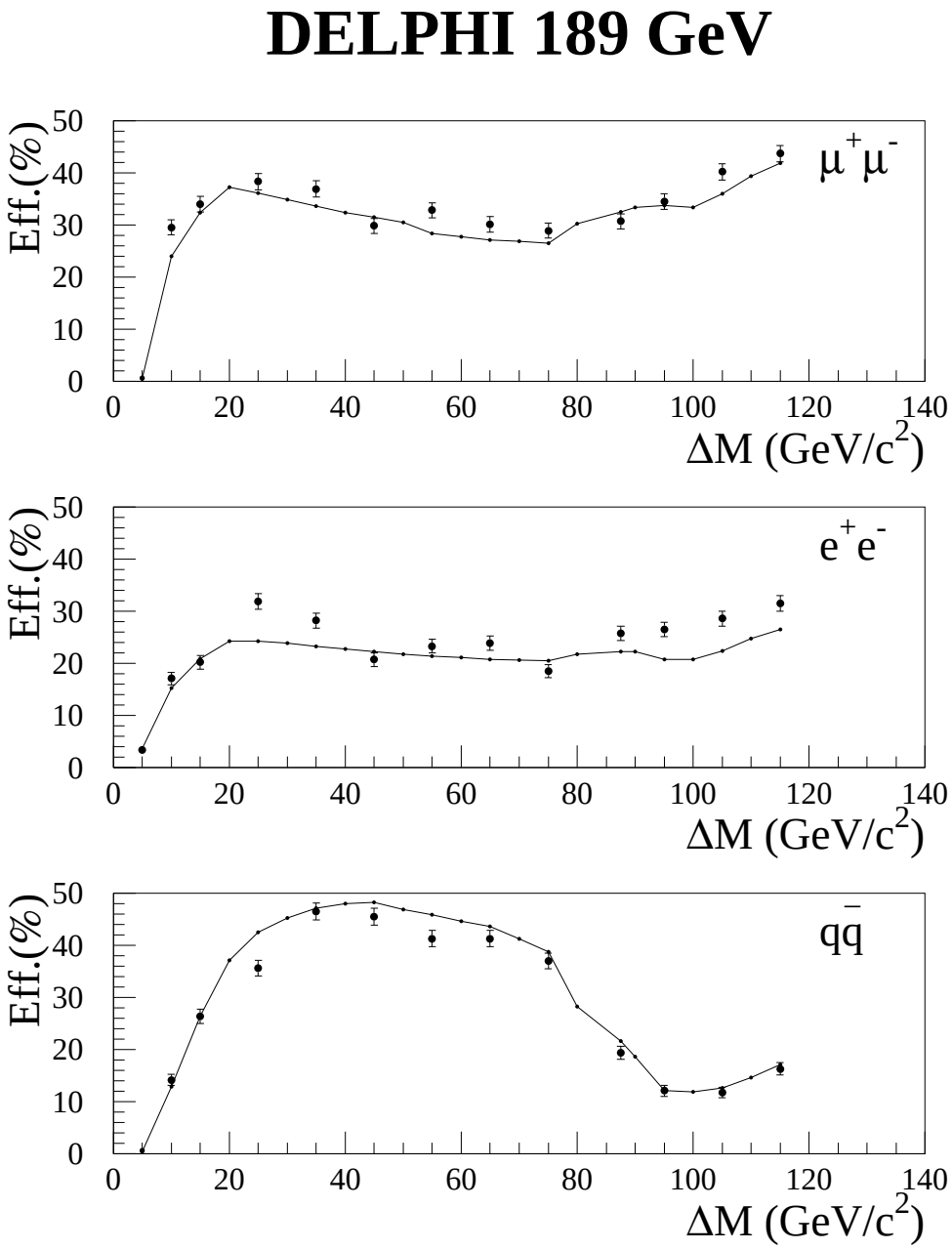

Figure 6: Efficiencies for $\tilde{\chi}_1^0\tilde{\chi}_i^0$ production as obtained with the full simulation (`DELSIM`, points with error bars) and the fast simulation (`SGV`, points connected by straight lines) for different $\Delta M = M_{\tilde{\chi}_i^0} - M_{\tilde{\chi}_1^0}$, assuming the decays $\tilde{\chi}_i^0 \to \tilde{\chi}_1^0 \mathrm{f}\bar{\mathrm{f}}$ (f=μ,e,q). The mass of $\tilde{\chi}_1^0$ was fixed to 35 GeV/c^2.

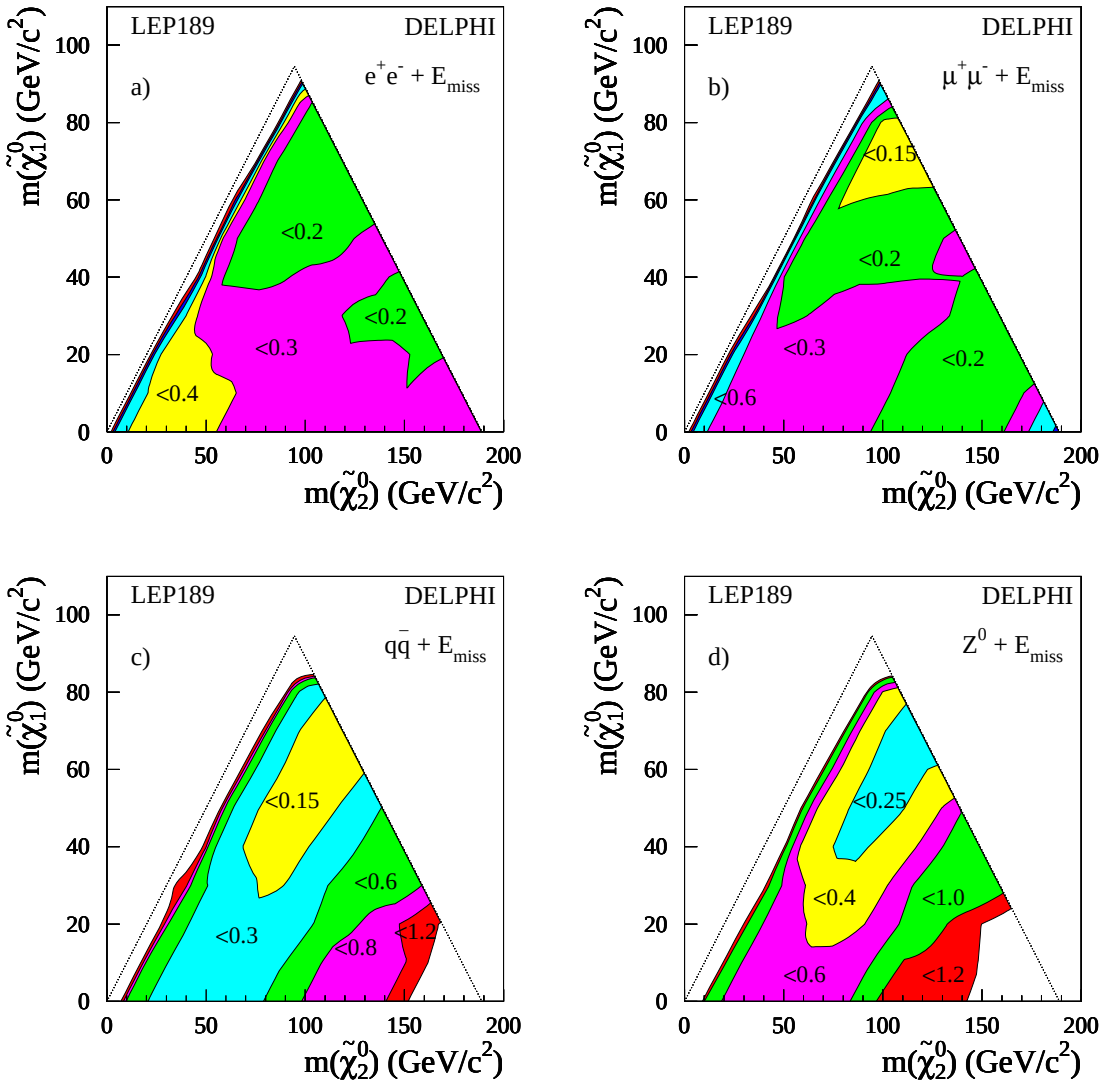

Figure 7: Contour plots of upper limits on the cross-sections at the 95% confidence level for $\tilde{\chi}_1^0\tilde{\chi}_2^0$ production at $\sqrt{s} = 189$ GeV. In each plot, the different shadings correspond to regions where the cross-section limit in picobarns is below the indicated number. For figures a), b), c), $\tilde{\chi}_2^0$ decays into $\tilde{\chi}_1^0$ and a) e^+e^-, b) $\mu^+\mu^-$, and c) $q\bar{q}$, while in d) the branching ratios of the Z was assumed, including invisible states. The dotted lines indicate the kinematic limit and the defining relation $M_{\tilde{\chi}_2^0} > M_{\tilde{\chi}_1^0}$.

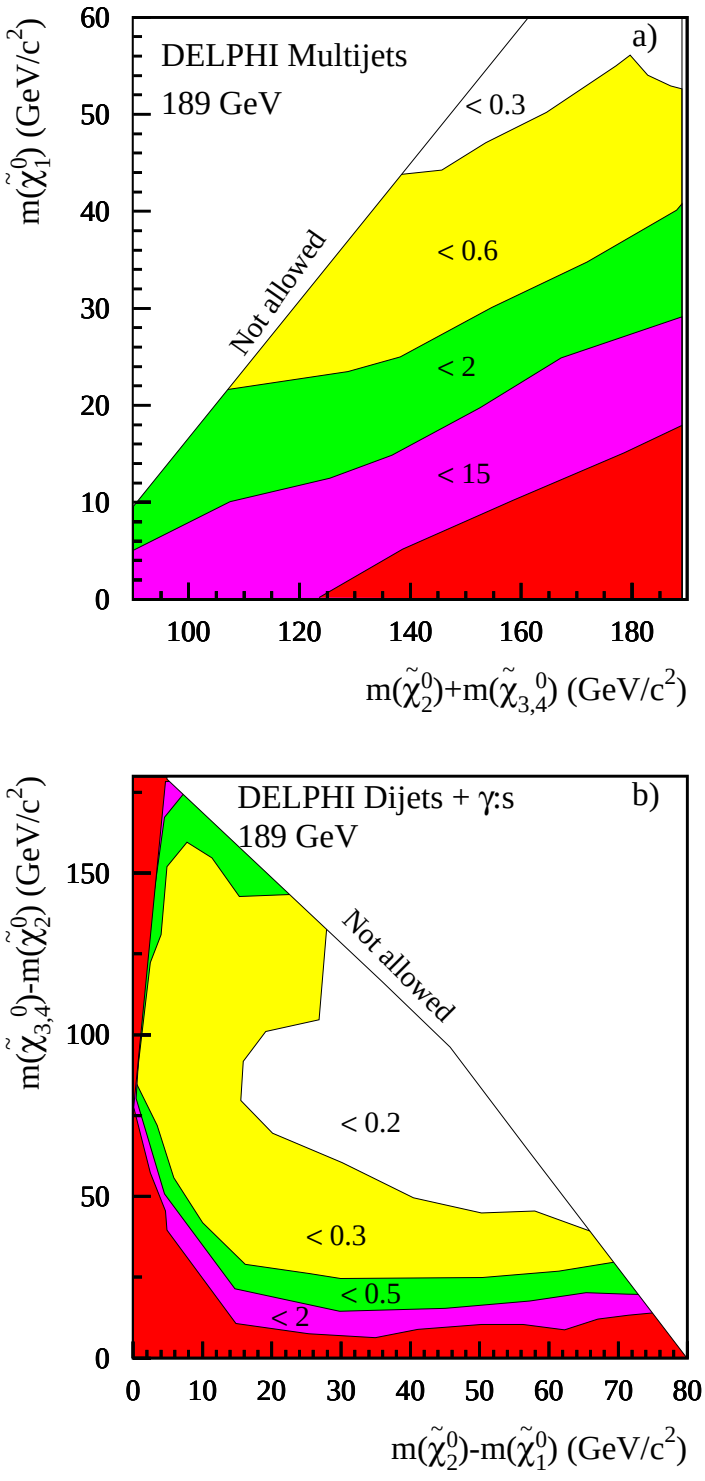

Figure 8: Upper limits on the cross-sections at the 95% confidence level for $\tilde{\chi}_2^0\tilde{\chi}_i^0$ production with $\tilde{\chi}_i^0 \to \tilde{\chi}_2^0 q\bar{q}$ (i=3,4) at $\sqrt{s} = 189\,\text{GeV}$. The different shades correspond to regions where the cross-section limit in picobarns is below the indicated number. In the darkest shaded regions there are points which are not excluded for any cross-section. $\tilde{\chi}_2^0$ was assumed to decay into $\tilde{\chi}_1^0 q\bar{q}$ in a), and into $\tilde{\chi}_1^0\gamma$ in b). The limits in a) are based on the acoplanar jets and multijets selections, while those in b) derive from the search for multijets with photons.

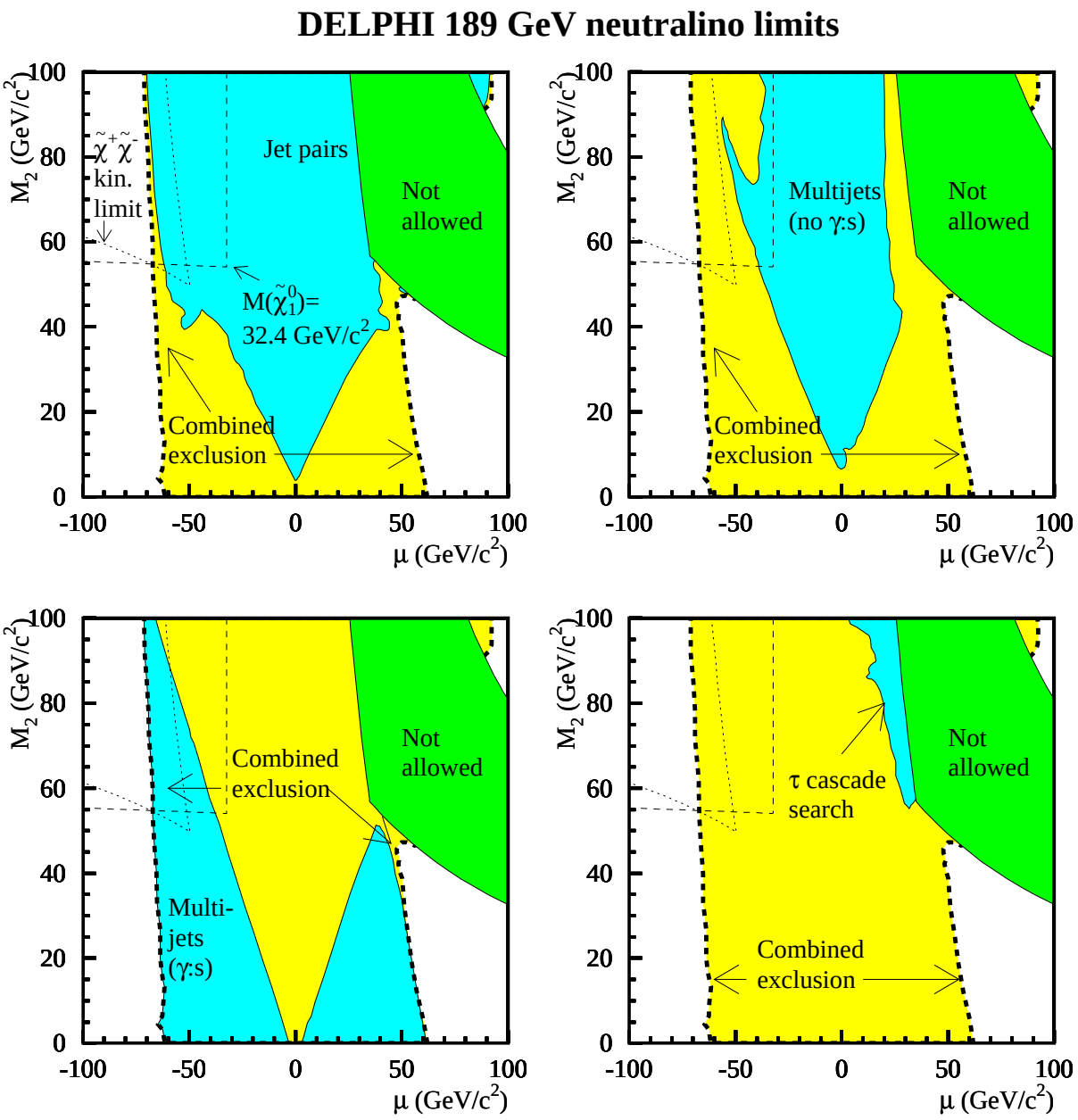

Figure 9: Regions in the (μ, M_2) plane excluded at 95% confidence level for $\tan\beta$=1, assuming $m_0 = 1$ TeV/c^2. The exclusion by individual searches for jet pairs (top left), multijets without γ:s (top right), multijets with γ:s (bottom left), and τ cascades (bottom right) are compared with the combined exclusion based on all searches (thick dashed curve and light shading). Also shown are the kinematic limit for chargino production (thin dotted curve) and the isomass contour for the minimum allowed neutralino mass [1] (thin dashed curve). In the region marked "Not allowed" the chargino is the LSP.

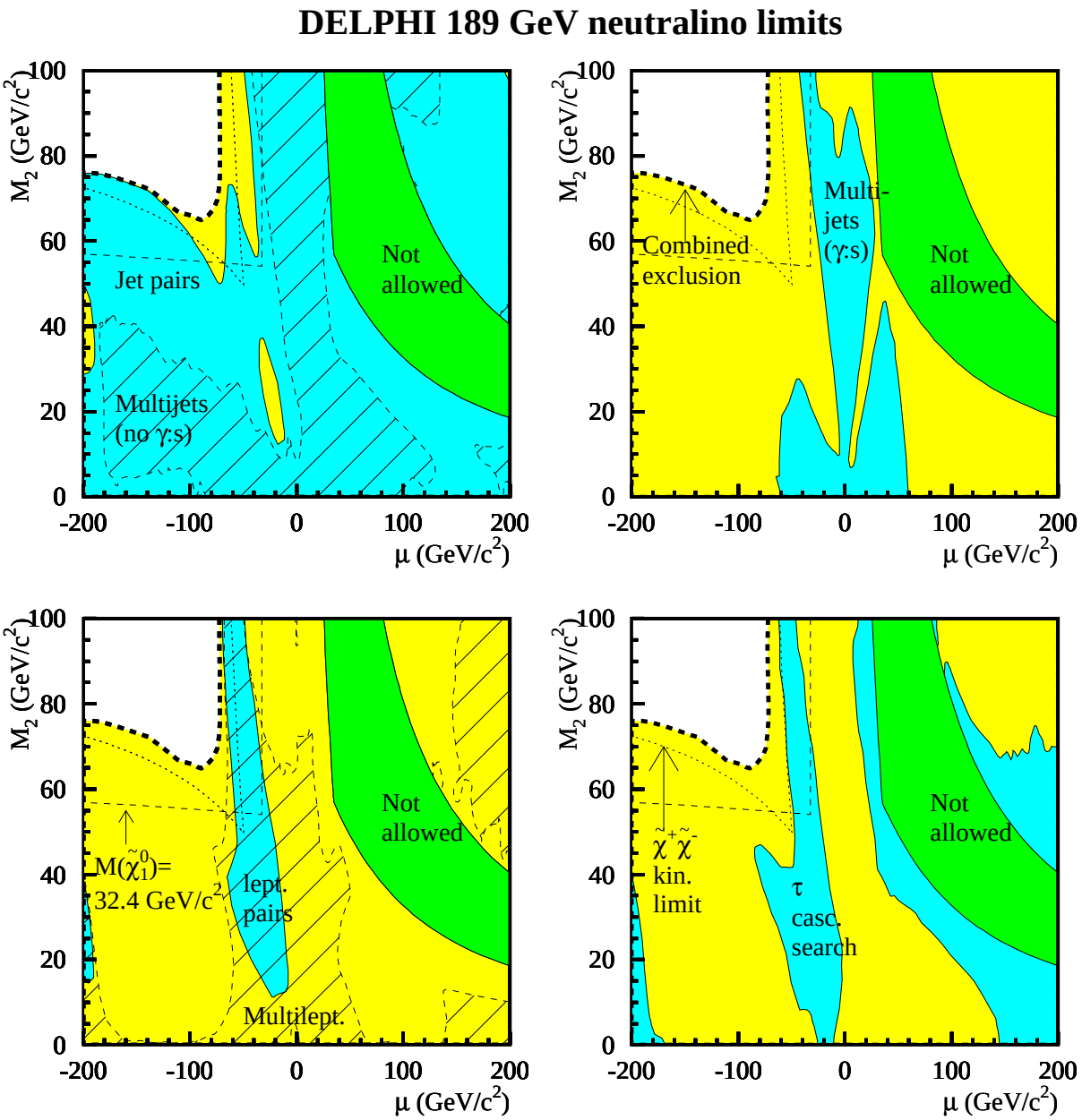

Figure 10: As figure 9, but for $m_0 = 80$ GeV/c^2 and six different contributing searches. From left to right and top to bottom: jet pairs and multijets without γ:s (hatched), multijets with γ:s, lepton pairs and multileptons (hatched), and τ cascades.